Performance comparison of equalization techniques for SI-POF multi-gigabit communication with PAM-M and device non-linearities

Performance Comparison of Equalization Techniques for SI-POF Multi-Gigabit with PAM-*M* and Device Non-linearities

Isaac N. Osahon*, Sujan Rajbhandari** and Wasiu O. Popoola*

*School of Engineering, Institute for Digital Communications, LiFi Research and Development Centre
University of Edinburgh, EH9 3JL, UK.

**Centre for Mobility and Transport, School of Computing, Electronics and Mathematics,
Coventry University, CV1 2JH, UK.

Email: {i.osahon@ed.ac.uk, sujan.rajbhandari@coventry.ac.uk and w.popoola@ed.ac.uk}

***Abstract*—In this paper, Gigabit per second transmission over short-range step-index plastic optical fibre (SI-POF) is implemented with multi-level pulse amplitude modulation (PAM-*M*) scheme using a laser diode (LD) as the optical source. In particular, the POF channel distortion and the non-linear distortion from the LD are considered. To mitigate these distortions under various PAM-*M* levels, the bit error rate (BER) performances of the transversal, Volterra and multi-layer perceptron (MLP) based decision feedback equalizers are evaluated and compared. Furthermore, the inverse polynomial technique for non-linear mitigation is also considered. MLP is shown to offer the best BER performance for PAM scheme using more than 8 levels especially for a system with high non-linearities. With the MLP equalizer, we record the highest data rate of 3 Gbps, 7.8 Gbps and 18 Gbps for POF lengths of 60 m, 30 m and 10 m respectively.**

***Index Terms* - Polymer optical fibre (POF), multilayer perceptron (MLP), non-linear equalization, pulse amplitude modulation (PAM), non-linearity**

I. Introduction

In recent years, there has been an increasing interest in step-index plastic optical fibre (SI-POF) for use in short-range optical communications for in-home and automotive networks due to its low cost, ease of installation and handling, resilience to electromagnetic interference, and low weight [1], [2].

However, Gigabit transmission over SI-POF using intensity modulation and direct detection (IM/DD) usually suffers from channel distortion resulting in inter-symbol interference (ISI). This has lead to an intensive research in different spectrally efficient modulation schemes suitable for the IM/DD channel. These modulation schemes include multi-level pulse amplitude modulation (PAM-M), carrierless amplitude and phase (CAP) modulation and orthogonal frequency division multiplexing (OFDM). Due to its simplicity, PAM-M is considered as an attractive modulation scheme for IM/DD systems and it has been shown to outperform OFDM [3]. With the aid of post equalizers, PAM-M has been demonstrated to be suitable for Gigabit transmission [4], [5].

The common optical sources for SI-POF (and fibre/ free space optic communication in general) are the laser diodes (LDs) and the light emitting diodes (LEDs). LDs are expensive than LEDs but they offer higher modulation bandwidth and optical power. While most commercial LEDs offer modulation bandwidth ranging from 3 MHz to 400 MHz and optical power less than 2 mW, the conventional LDs can offer over 1 GHz modulation bandwidth with an optical power of up to 20 mW [3], [6]. Consequently, 5 Gbps transmission over 50 m SI-POF was reported with an LD using PAM-M and post- equalization [7] while the same data rate was achieved with LED for 10 m SI-POF [4]. However, major drawbacks of an LD include its low reliability and high sensitivity to changes in temperature. Moreover, the conversion of the input current to optical power from the LD (and also LED) is non-linear, which gives rise to non-linear distortions in the received signal. The effects of this non-linearity are significant for high-order multi-level modulation formats.

The channel distortion due to ISI is usually mitigated with the conventional transversal (or FIR-filter) based equalizers. However, these equalizers are not optimum for a non-linear system. Hence, three major solutions have been reported in previous studies to reduce the effect of the system non-linearities [3]. One is by applying non-linear pre-distortion techniques, the popular one being the inverse non-linear polynomial pre-distorter [8]. This method applies the inverse non-linear polynomial of the LD/LED response to the signal before IM so that the overall response of the system is linear. The second solution is with Volterra equalizers, which is similar to the transversal equalizer except that it involves computing the Volterra inputs before equalization [9]. Artificial neural network (ANN) based equalization is the third approach for mitigating ISI as well as the system non-linear distortions and multilayer perceptron (MLP) is one of such ANN used for channel equalization [10]–[12].

Therefore, the specific contributions from this work are as follows:

1) the LD's behaviour with respect to non-linear distortions when using PAM-M scheme are examined and
2) a comprehensive comparison of the three approaches (transversal, Volterra and MLP) in mitigating both ISI and non-linearity is presented in this paper for the first time. The channel used in this study is based on

real SI-POF experimental measurements. The results suggest that the MLP equalizer is the best option for a non-linear system especially one with higher level modulation format.

II. System Model Description

A. Experimental Setup

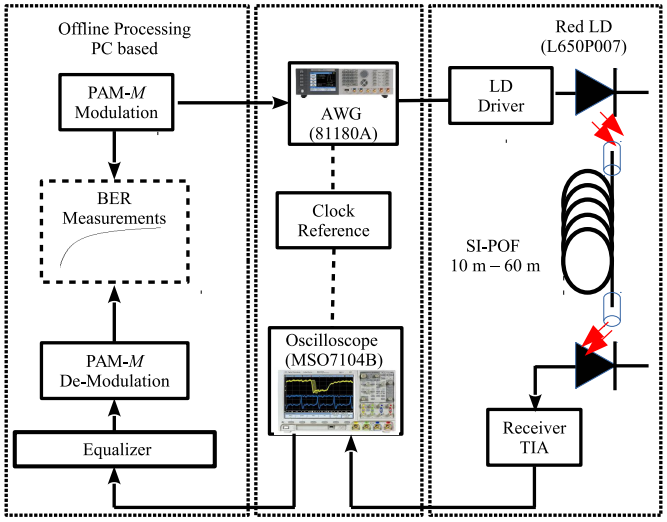

Fig. 1. Diagram illustrating the experiment setup

The setup for subsequent experiments in this study is illustrated in Fig. 1. A pseudorandom binary sequence (PRBS) data of a length of $2^{20}-1$ is generated offline using a computer in Matlab environment. The binary data is PAM-M modulated by mapping $\log_2(M)$ bits to one of M amplitude levels with gray coding. The data symbols are preceded by a preamble of 4000 symbols that is used for synchronization at the receiver and for training the equalizer. The resulting symbol sequence is upsampled and fed through a digital pulse shaping filter. In this study, a root-raised-cosine filter with a roll-off factor of 0.5 is used. The modulated and pulse shaped signal is then loaded to an arbitrary waveform generator (AWG, Keysight 81180A, 12 bits digital-to-analogue converter (DAC) resolution, 1 GHz bandwidth, 4.2 Gsa/s sampling rate). The output of the AWG is a bipolar voltage signal used as an input to a laser driver to drive the red 650 nm LD (L650P007). The measured electrical-to-optical (E/O) conversion of the LD is defined by its optical power-to-electrical current (P-I) curve shown in Fig. 2. The AWG's output voltage signal is converted to a unipolar current signal with the addition of DC voltage via a Bias-T (ZFBT-4R2GW+). The bias current (I_{bias}) is ∼30 mA, which translates to an average optical fibre-coupled power is ∼8 mW from the P-I curve. Furthermore, the peak modulating current to the LD (I_{mod}) is set as 7 mA. The output of the red LD is transmitted through a SI-POF (HFBR-RUD500Z) with a measured attenuation of ∼0.18 dB/m at 650 nm wavelength. The optical signal from the SI-POF is then received by a photo-receiver (New Focus Model 1601, 1 GHz bandwidth) and the output electrical signal from the receiver is captured

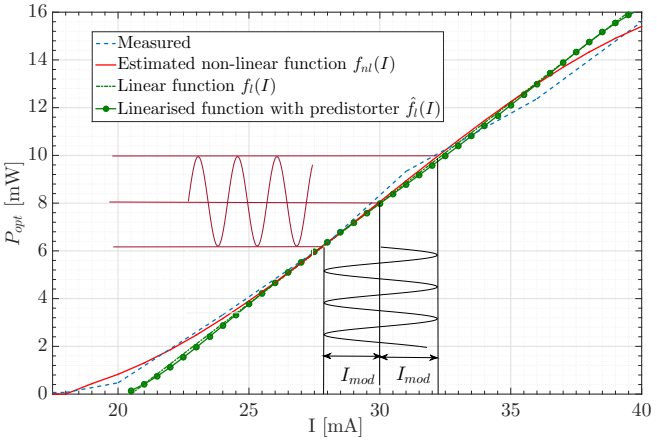

Fig. 2. Measured and estimated P-I curve of the LD (L650P007)

with an oscilloscope (MSO7104B, 1 GHz bandwidth, 4Gsa/s, 8 bits vertical resolution). The captured signal is then imported into the computer for post-processing, which comprises of matched filtering, down-sampling and equalization. Finally, the equalized signal is demodulated, thus offering the received binary data, which in turn is compared with the transmitted binary data to obtain the bit error rate (BER).

B. Simulation Model

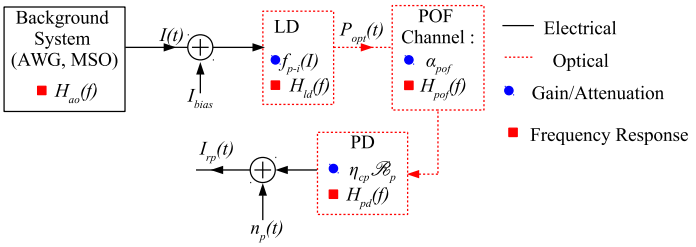

Fig. 3. Model illustration of the POF system

An equivalent block diagram for simulating the experiment in Section II-A is shown in Fig. 3. A constant upsampling factor of 4 is used for the simulation model irrespective of the signal's data rate. From Fig 3, the output signal $I_{rp}(t)$ is given as:

$$I_{rp}(t) = \mathscr{R}_p \eta_{cp} \alpha_p (|x_{opt}(t) \otimes h_{pch}(t)|^2) + n_p(t), \quad (1)$$

where $\mathscr{R}_p$ denotes the photodiode (PD) responsivity in A/W. η_{cp} denotes the maximum coupling efficiency and this is significant when the radius of the POF cable (r_{pof}) is above the radius of the PD (r_{pd}), so $\eta_{cp} = \left(\frac{r_{pd}}{r_{pof}}\right)^2$; α_p is the attenuation of the POF channel and $\alpha_p = 10^{-0.1\times\alpha_{pc}\times l_p}$ where l_p is the POF length in metres and α_{pc} is the POF attenuation coefficient in dB/m. $x_{opt}(t)$ denotes the optical signal field from the LD and the optical power $P_{opt}(t) = |x_{opt}(t)|^2$. $P_{opt}(t)$ is obtained from the P-I curve function that is shown

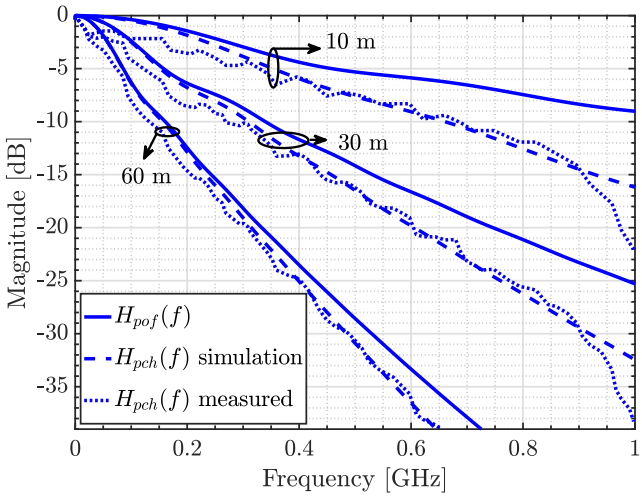

Fig. 4. The magnitude response of the system under various SI-POF length. $H_{pof}(f)$ is generated with the power flow model using the HFB profile [13].

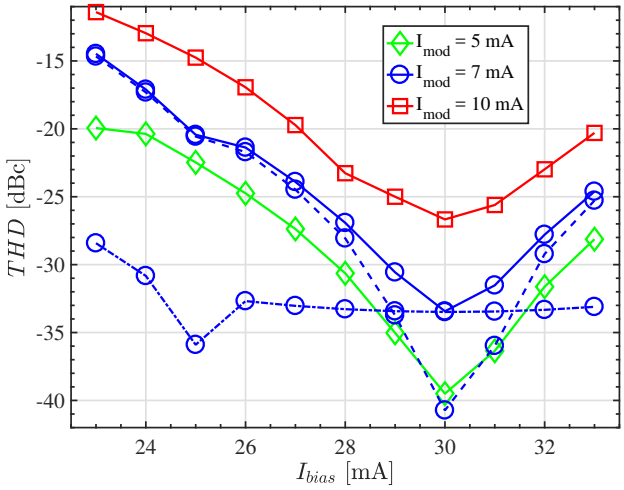

Fig. 5. Total harmonic distortion (THD) at the LD output for various I_{mod}. For I_{mod} = 7mA, the dashed and dash-dotted lines denote the second and third harmonic distortion respectively.

in Fig. 2. The non-linear P-I transfer function $f_{nl}(.)$ is given as:

$$f_{nl}(I) = \begin{cases} a_3 I^3 + a_2 I^2 + a_1 I + a_0 & I > 18.9 \\ 0 & \text{otherwise} \end{cases}$$
$$\text{where } a_3 = -0.001414, a_2 = 0.1278, a_1 = -2.98, \quad a_0 = 20.62. \tag{2}$$

In (1), $h_{pch}(t)$ denotes the impulse response of the overall channel, which consists of the background system (AWG and oscilloscope) and the POF system (LD, POF and receiver). The combined response of the AWG and oscilloscope was measured and can be represented as a 1^{st} order Butterworth lowpass filter with a 3 dB bandwidth of 800 MHz. LDs generally have bandwidth ranging from few GHz to tens of GHz [14], so the response of the LD can be assumed to be flat within the overall system bandwidth. The POF channel response, on the other hand, can be represented with various models. One of these models is the Gaussian response and it is a useful estimate for POF of longer length (usually above 100 m). For shorter POF lengths however, the power flow equation is a better model for estimating the SI-POF channel response [15]. With the power flow model, the magnitude response of the SI-POF for lengths of 10 m, 30 m and 60 m is depicted in Fig. 4. A detailed description of the power flow model is shown in [13], [15], [16]. The PD's response is estimated with 1^{st} order Butterworth lowpass filter with a 3 dB bandwidth of 1 GHz. Consequently,

$$h_{pch}(t) = h_{ao}(t) \otimes h_{pof}(t) \otimes h_{pd}(t), \tag{3}$$

where $h_{ao}(t)$ is the combined impulse response for the AWG and oscilloscope; $h_{pof}(t)$ is the impulse response for the SI-POF channel; and $h_{pd}(t)$ is the impulse response for the receiver. To validate this simulation model, Fig. 4 shows and compares the frequency response of $h_{pch}(t)$ from simulation and experiment for the three different SI-POF lengths. It is observed that the frequency response from the model matches that of the experiment.

The noise, denoted by $n_p(t)$, is the additive white Gaussian noise (AWGN) at the receiver. It is assumed here that the dominant noise source is derived from the receiver's sensitivity and the shot noise. Thus, the noise variance can be written as:

$$N_p = B_{np}\left((\mathscr{R}_p \mathscr{N}_{nep})^2 + 2q\mathscr{R}_p \alpha_p \eta_{cp} P_{avg}\right), \tag{4}$$

where $\mathscr{N}_{nep}$ is the noise equivalent power (NEP) of the receiver in W/$\sqrt{\text{Hz}}$, q is the quantity of charge for an electron ($1.6 \times 10^{-19} C$), and P_{avg} is the mean of the optical signal $P_{opt}(t)$. B_{np} is the effective noise bandwidth of the channel, which is defined as the bandwidth of a brick-wall filter that has the same power (or energy) as the channel [17]. This can be obtained as:

$$B_{np} = \int_0^\infty |H_{psf}(f) H_{pch}(f)|^2 \, df, \tag{5}$$

where $H_{psf}(f)$ represents the frequency response of the pulse shaping filter.

C. Estimated SNR per bit for the SI-POF link

The estimated signal-to-noise ratio (SNR) per bit (γ) in dB can be computed as a function of the data rate (R_b) in Gbps and the number of PAM levels (M) as [15]:

$$\gamma = \gamma_{nm} - 10\log_{10}\left(\frac{3R_b(M-1)}{M+1}\right)$$
$$\gamma_{nm} = 10\log_{10}\left(\frac{(\alpha_p \eta_{ld} I_{mod} \eta_{cp} \mathscr{R}_p)^2}{(\mathscr{R}_p \mathscr{N}_{nep})^2 + 2q\mathscr{R}_p \alpha_p \eta_{cp} P_{avg}}\right) - 90, \tag{6}$$

where η_{ld} denotes the slope efficiency (or electrical current-to-optical power conversion ratio) and is estimated from Fig. 2 as 0.8. The average transmitted optical power P_{avg} is obtained as $P_{avg} = \eta_{ld}(I_{bias} - 20)$. γ_{nm} is the normalised SNR per bit that is independent of R_b and M. The expression in (6) is only valid if ISI and the non-linear penalties are ignored.

D. Non-linear Signal Distortions from the Laser Diode

In Fig. 5, the total harmonic distortion (THD) at the LD output is computed with respect to I_{mod} and I_{bias}. The THD in dBc is defined as:

$$THD = 10\log_{10}\left(\frac{1}{P_1}\sum_{n=2}^{\infty} P_n\right), \tag{7}$$

where P_n is the power (in Watts) for the n^{th} harmonic with $n = 1$ being the fundamental frequency. The THD is obtained by measuring the power of the first five harmonics using a fundamental frequency of 40 MHz. To maximize the SNR at the transmitter, a high I_{mod} is desirable as shown in Section II-C. However, it is seen in Fig. 5 that the non-linear distortion from the LD increases with I_{mod}. Also, there is an optimum value of I_{bias} that offers the minimum THD of the LD. It is important that I_{bias} does not exceed this value as it would not only increase the THD of the LD but also reduce the lifetime of (or even damage) the LD. The minimum THD for $I_{mod} = 5\ mA$ and $I_{mod} = 10\ mA$ is about -39 dBc and -27 dBc respectively with $I_{bias} = 30\ mA$.

E. Inverse polynomial pre-distorter model

The relation between the input current and the optical power for the LD is modelled as the 3$^{\text{rd}}$ degree polynomial function $f_{nl}(I)$ expressed in (2). The function shows that the current range for the LD is within the range of ∼19 mA up to ∼40 mA. The pre-distorter linearises $f_{nl}(I)$ by using the inverse polynomial function $f_{nl}^{-1}(I)$ and a linear function $f_l(I)$. The polynomial function for the pre-distorter can, therefore, be obtained as [8]:

$$\begin{aligned} f_{pred}(I) &= f_{nl}^{-1}(f_l(I)), \\ \text{where } f_l(I) &= 0.8421I - 17.26, \\ \text{and } f_{nl}^{-1}(I) &= 0.005623I^3 - 0.14I^2 + 2.247I + 18.07. \end{aligned} \tag{8}$$

The output of the pre-distorter is then passed through the LD to obtain the linearised response ($\hat{f}_l(I)$). It is shown in Fig. 2 that the linearised function from the pre-distorter $\hat{f}_l(I)$ matches the linear function $f_l(I)$. However, the current range that can be modulated linearly is from ∼ 20.5 mA to ∼37 mA.

F. Multi-Gigabit Transmission with PAM-M and Equalization

Due to the bandwidth limitation of the SI-POF channel, transmission of data at multi-gigabit per seconds speed with PAM-M results in ISI, which can be mitigated with equalization. In this study, $M \in \{4, 8, 16, 32\}$ is considered and the value of the common parameters used in this study are provided in Table I.

Furthermore, three different symbol-spaced decision feedback equalizers (DFEs) are examined in this study and they are: the transversal DFE (TRDFE), the 2^{nd} order Volterra DFE (VOLT2DFE) and the MLP based DFE (MLPDFE). More details on these DFEs can be explored in [18]–[22]. For the purpose of equalization, MLP requires at least three layers (input layer, one hidden layer, output layer) [20], [22].

TABLE I
SETUP PARAMETERS

Parameters	Symbol	Values
POF attenuation coefficient	α_{pc}	0.18 [dB/m]
POF PD responsivity @ 650 nm	$\mathscr{R}_p$	0.45 [A/W]
POF radius	r_{pof}	0.5 [mm]
PD Radius	r_{pd}	0.2 [mm]
Receiver NEP @ 650 nm	$\mathscr{N}_{nep}$	35 [pW/$\sqrt{\text{Hz}}$]
Equalizer number of forward taps	N_{ft}	22
Equalizer number of feedback taps	N_{bt}	18
Equalizer number of training examples	N_{tr}	4000
Number of bits for BER testing	N_{bit}	10^6

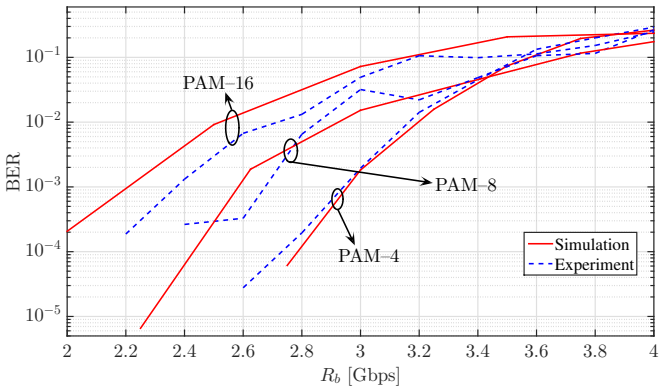

Fig. 6. BER plot for $M \in \{4, 8, 16\}$ comparing the results from simulation with those of experiment using the transversal DFE. $l_p = 60$ m, $I_{bias} = 30$ mA, $I_{mod} = 7$ mA

So the number of layers for the MLPDFE in this study is three. The recursive least squares (RLS) algorithm, with a forgetting factor of 1, is used to train both the transversal and the Volterra DFE while the Levenberg-Marquardart back-propagation (LMBP) algorithm is used for the MLPDFE. After training, no adaptive algorithm is employed for the DFEs so that their tap weights are kept constant. The number of training examples in Table I is sufficient for the DFEs except for MLPDFE which requires more training examples to further improve its performance. The optimum number of taps for the DFEs vary depending on the PAM level and the data rate. However, the number of taps from Table I is obtained by doing an extensive search with TRDFE to find the minimum number of taps that maximizes the data rate at a BER of 10^{-3} with PAM–4 scheme using the 60 m POF.

The computational complexity of the equalizers (with and without the algorithm) is compared and presented in Table II. The average training time is computed for $N_{tr} = 4000$ with MATLAB using a computer with Intel®Xeon®Processor E5-1660 v3 @ 3.00 GHz. The values from Table II suggests that if $N_{hn} \ll (N_{ft} + N_{bt})$, then VOLT2DFE has higher computational order than the MLPDFE. Also, the TRDFE is the least complex of the three equalizers considered.

TABLE II
COMPLEXITY COMPARISON OF THE EQUALIZATION SCHEMES

Equalizer	Training algorithm	Number of input taps (or synaptic weights)	Complexity of Equalizer:		Average training time(seconds)
			with training algorithm	without training algorithm	
TRDFE	RLS	$N_t = N_{ft} + N_{bt}$	$O(N_t^2)$	$O(N_t)$	0.532
VOLT2DFE	RLS	$N_{2t} = 0.5N_{ft}^2 + 1.5N_{ft} + N_{bt}$	$O(N_{2t}^2)$	$O(N_{2t})$	17.628
MLPDFE	LMBP	$W = N_{hn}(N_{ft} + N_{bt} + 2)$	$O(W^2 + WN_{tr})$	$O(W)$	4.028

– The computational complexity for TRDFE, VOLT2DFE and MLPDFE is derived from [18], [19] and [20] respectively.
– The number of hidden neurons for MLPDFE, denoted as N_{hn}, is six in order to compute the average training time.
– Unlike TRDFE and VOLT2DFE, MLPDFE has N_{hn} non-linear functions.

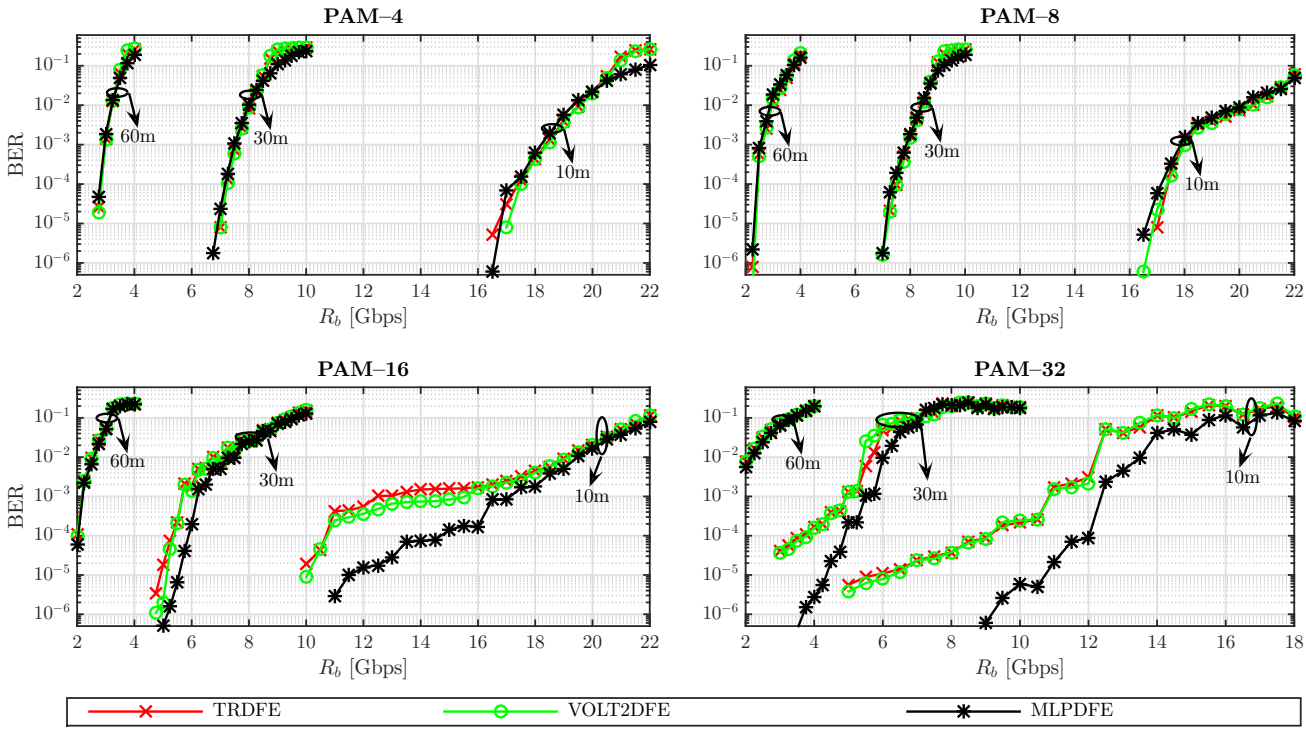

Fig. 7. BER result comparing the equalizers performance over SI-POF with LDS1 setup ($I_{bias} = 30$ mA, $I_{mod} = 7$ mA). γ_{nm} is ∼37 dB, ∼47 dB and ∼53 dB for SI-POF lengths of 60 m, 30 m and 10 m respectively.

III. RESULTS AND DISCUSSIONS

To evaluate and compare the performance of the equalizers in the presence of ISI and non-linearity, we present the BER results at various data rates for 60 m, 30 m and 10 m POF lengths. Each simulation result presented is the average of ten independent realisations. In order to assess the impact of the LD non-linearities, we consider two different setups for the input current signal to the LD. These are denoted as LDS1 and LDS2 in the rest of the paper. For LDS1, the input current signal is such that $I_{bias} = 30$ mA and $I_{mod} = 7$ mA, while for LDS2, $I_{bias} = 26$ mA and $I_{mod} = 7$ mA. LDS1 has the least non-linear distortion while LDS2 has the highest non-linear distortion as depicted in Fig. 5. Using (6) the average SNR per bit for $M = 4$ and $R_b = 3$ Gbps is estimated as 29 dB, 39 dB and 45 dB for 60 m, 30 m and 10 m POF lengths respectively.

In Fig. 6, the BER result from the simulation model in Section II-B is compared with that from the experiment setup in Section II-A for $M \in \{4, 8, 16\}$ using the LDS1 setup ($I_{bias} = 30$ mA, $I_{mod} = 7$ mA). The POF length is 60 m and the transversal DFE is used to obtain this BER result. It is observed that the simulation model provides a good estimate of the experiment for PAM–4 and PAM–8. At a BER of 10^{-3} for PAM–16, the data rate from the experiment is 0.2 Gbps higher than that from the simulation. Henceforth, the simulation model (described in Section II-B) would be used to assess and evaluate the performance of the SI-POF channel under LD non-linearities.

In Fig. 7, the BER result for the equalizers with the LDS1 setup ($I_{bias} = 30$ mA, $I_{mod} = 7$ mA) is depicted for POF lengths of 10 m, 30 m and 60 m. It should be noted here that for the LDS1 setup, there are 6 hidden neurons ($N_{hn} = 6$) for the MLPDFE for it to achieve the best performance while not compromising computational complexity. It is seen for the LDS1 that the highest data rate obtained at a BER of 10^{-3}

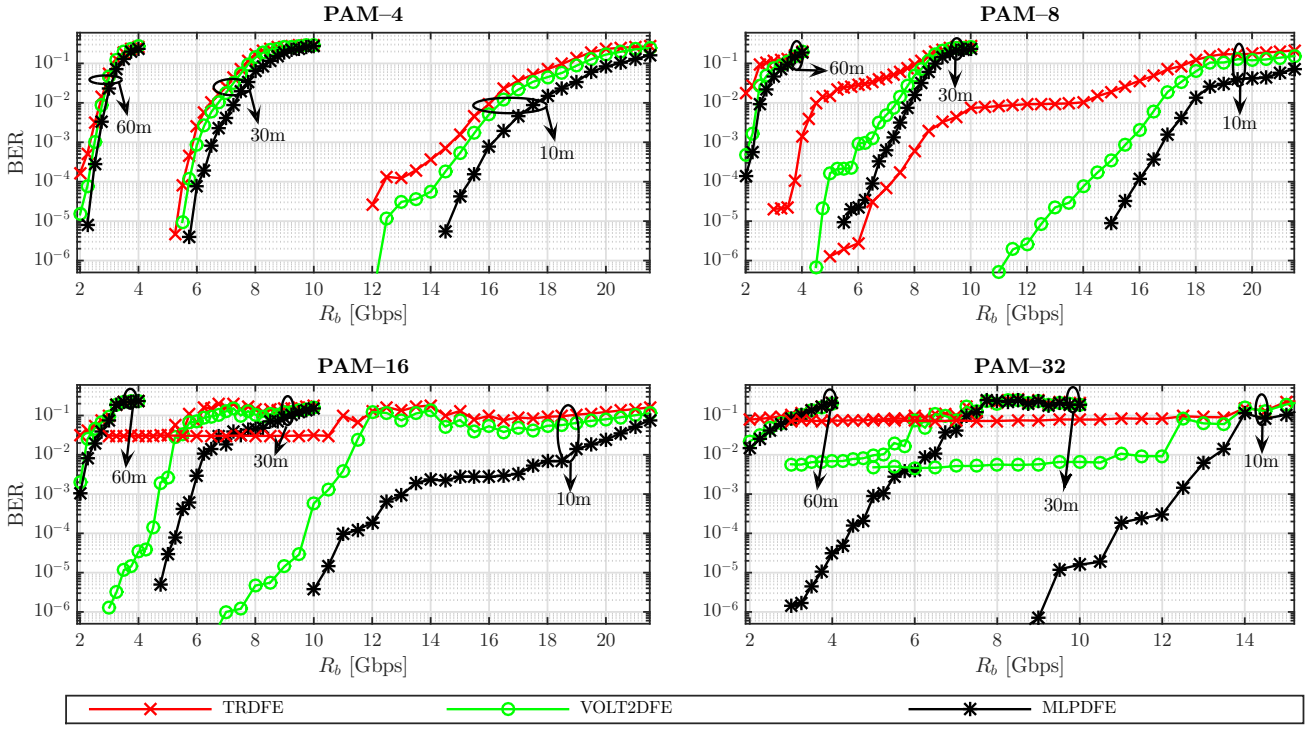

Fig. 8. BER result comparing the equalizers performance over the SI-POF with the LDS2 setup ($I_{bias} = 26$ mA, $I_{mod} = 7$ mA). γ_{nm} values are similar to those in Fig. 7

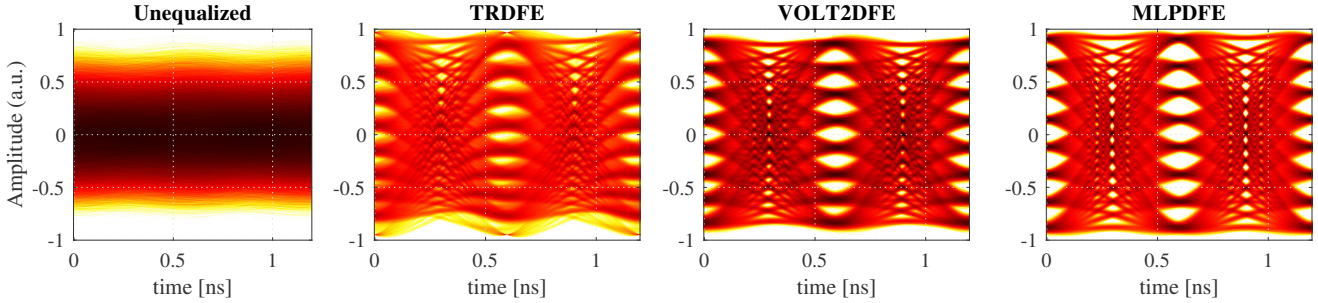

Fig. 9. Computed eye diagram for PAM–8 at 5 Gbps over 30 m SI-POF using the setup in Fig. 8

with the three DFEs is ∼3 Gbps for 60 m POF with PAM–4, ∼7.8 Gbps for 30 m POF with PAM–8, and ∼18 Gbps for 10 m POF with PAM–8. Also, the three DFEs offer similar BER for $M \leq 8$. This is because the non-linear distortion is minimal for the LDS1 setup with negligible effect at lower modulation order. The optimum PAM scheme with the LDS1 setup is PAM–4 for 60 m POF and PAM–8 for both 30 m and 10 m POF. With $M > 8$ however, the MLPDFE BER performance is superior to both VOLT2DFE and TRDFE for 10 m and 30 m POF lengths. For example, with PAM–16 ∼6.2 Gbps data rate is achieved with MLPDFE at a BER of 10^{-3}, while the other DFEs offer ∼5.7 Gbps for a 30 m POF. Similarly for a 10 m POF with PAM–16, ∼17 Gbps data rate is obtained with MLPDFE, while this is ∼16 Gbps with the other DFEs. For PAM–32, the achievable data rate at 30 m is ∼5.7 Gbps with MLPDFE while it is ∼5.2 Gbps with both VOLT2DFE and TRDFE. For 10 m POF with PAM–32, this is ∼12.3 Gbps with MLPDFE while it is ∼10.8 Gbps with the other DFEs.

With higher amount of non-linear distortion represented as LDS2 setup ($I_{bias} = 26$ mA, $I_{mod} = 7$ mA), the BER against data rate results are presented in Fig. 8. Unlike with the LDS1 setup, 24 hidden neurons ($N_{hn} = 24$) is used for the MLP's optimal performance with the LDS2 setup since it has more non-linear distortion than the LDS1 setup. It is observed in Fig. 8 that the highest data rate achieved at a BER of 10^{-3} with the TRDFE is ∼2.3 Gbps for 60 m, ∼5.8 Gbps for 30 m, and ∼14.3 Gbps for 10 m POF with PAM–4 scheme used for all the POF lengths. For VOLT2DFE, the values are 2.5 Gbps for 60 m with PAM–4, 6.25 Gbps for 30 m with PAM–8, and ∼15.6 Gbps for 10 m with PAM–8. For MLPDFE, this is ∼2.8 Gbps for 60 m with PAM–4, ∼7.2 Gbps for 30 m with PAM–8, and ∼16.8 Gbps for 10 m with PAM–8. Furthermore, there is no reliable transmission when the TRDFE

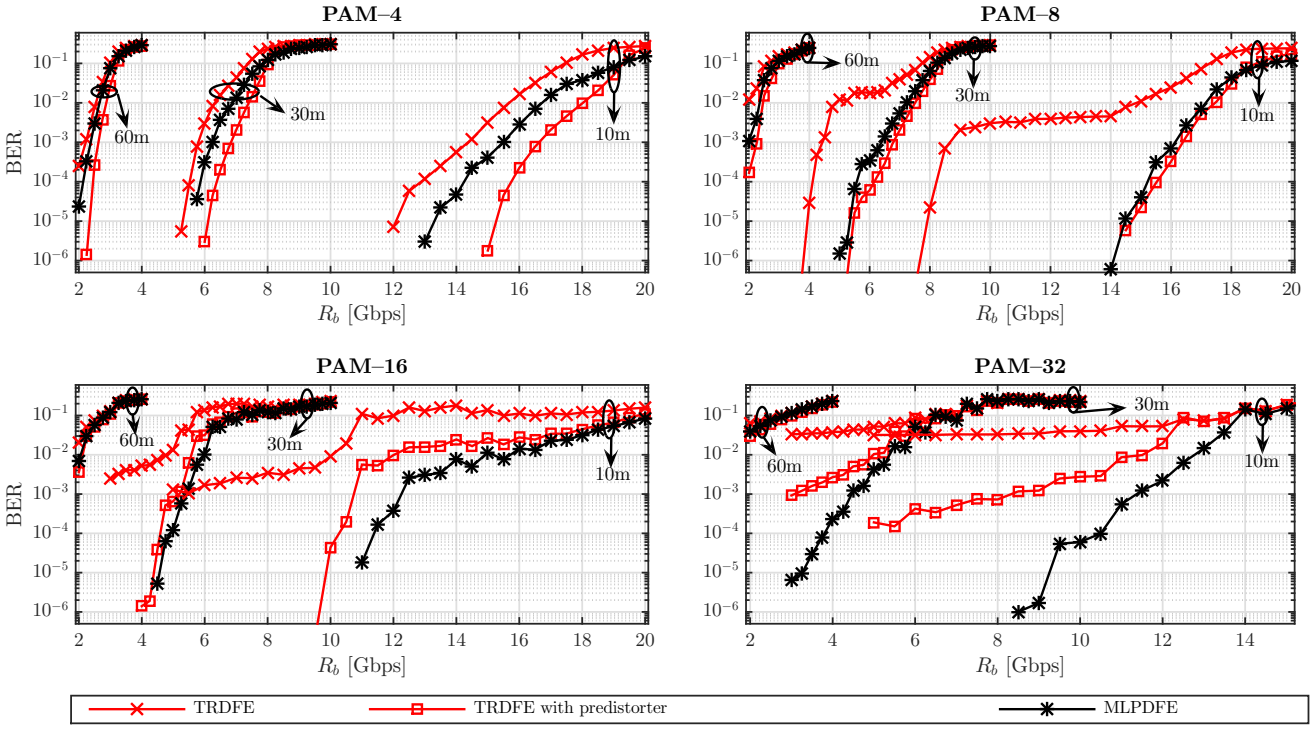

Fig. 10. BER result comparing the performance of MLPDFE with that of TRDFE with non-linear pre-distortion ($I_{bias} = 26$ mA, $I_{mod} = 5$ mA). γ_{nm} is $\sim$34 dB, $\sim$44 dB and $\sim$49 dB for SI-POF lengths of 60 m, 30 m and 10 m respectively.

is used with $M \in \{16, 32\}$ as the BER is greater than 0.02. This is higher than the forward error correction (FEC) limit of 3.8×10^{-3}. Also, for VOLT2DFE, the BER is always higher than FEC limit with PAM–32. This is however not the case with MLPDFE for all data rates considered with the exception of PAM–32 at 60 m POF length. Here, it can be inferred that in the presence of non-linear distortion, the MLPDFE is the most appropriate of the three equalizers. As an example, the eye diagrams for the output of each equalizer with PAM–8 scheme is shown in Fig. 9. The diagrams are computed for 30 m SI-POF at a data rate of 5 Gbps. Without equalization, the PAM–8 waveform is severely distorted due to ISI and the corresponding eye diagram is completely closed. With TRDFE, the eye diagram is opened but the levels are unequally spaced and this is because the equalizer does not mitigate the system non-linearity. More uniform spacing between levels is observed for the eye diagram with VOLT2DFE and MLPDFE as they compensate for the non-linearity inherent in the system. Moreover, the eye spacing with MLPDFE ($\gtrapprox$ 0.155 a.u.) is greater than that of VOLT2DFE ($\gtrapprox$ 0.070 a.u.) and this is evident in the BER plot in Fig. 8.

In Fig. 10, the BER result is used to compare the performance of the TRDFE that uses the inverse polynomial pre-distorter with that of the MLPDFE. I_{bias} is setup as 26 mA as this is the point on the LD with high non-linearity. Due to the limited current range of the pre-distorter as previously discussed in Section II-E, $I_{mod} = 5$ mA is used here. Similarly, 24 hidden layer neurons are used in the MLPDFE for it to achieve its best BER performance. Using the pre-distorter significantly improves the link performance especially at higher PAM levels. For $M \leq 8$, it is shown in Fig. 10 that when the TRDFE is used with the pre-distorter, it offers marginally better BER performance than the MLPDFE. For instance, the data rate at a BER of 10^{-3} offered by the MLPDFE is 15.5 Gbps for 10 m POF using PAM–4 scheme, but this is $\sim$16.2 Gbps with TRDFE using the pre-distorter. For $M > 8$ however, the MLPDFE outperforms the TRDFE even with the non-linear pre-distortion. There is still some non-linearity in the system with the pre-distorter. This is because the polynomial equation, from which the pre-distorter is obtained, is an approximation of the LD transfer function but not an exact expression.

From these results, it can be concluded that the MLP based equalizer offers the best mitigation against POF channel distortion and non-linearity. The Volterra equalizer only mitigates 2^{nd} order non-linearities so its BER performance is not as good as that of the MLP equalizer. The transversal equalizer on the other hand only mitigates the ISI and does not consider the non-linear distortion inherent in the system. Hence, it offers the least BER result. However, at lower PAM levels of M =4 and 8, the non-linear pre-distortion techniques with TRDFE is the best approach. For this study, the maximum data rates recorded are 18 Gbps for 10 m POF, 7.8 Gbps for 30 m POF and 3 Gbps for 60 m POF at a BER of 10^{-3}.

IV. Conclusion

We have experimentally demonstrated PAM-M transmission through an SI-POF and implemented post equalizers. A

simulation model is then developed based on the experimental setup. This model is then validated and shown to match the experiment results. The BER performances of the equalizers were considered in the presence of weak and strong non-linear distortions. From all investigated scenarios, the MLP equalizer offers the best performance especially for systems with high non-linear distortion and with higher PAM constellation ($M \geq 16$). Generally, higher PAM levels ($M \geq 16$) are attractive for high data rates but require high SNR and suffer from more non-linear distortion. With the MLP equalizer, a data rate of about 18 Gbps, 7.8 Gbps and 3 Gbps is achievable over 10 m, 30 m and 60 m of SI-POF respectively at the FEC limit.

REFERENCES

[1] A. Koonen and E. Tangdiongga, "Photonic home area networks," *Journal of Lightwave Technology*, vol. 32, no. 4, pp. 591–604, 2014.

[2] Y. Shi, E. Tangdiongga, A. Koonen, A. Bluschke, P. Rietzsch, J. Montalvo, M. M. de Laat, G. N. Van Den Hoven, and B. Huiszoon, "Plastic-optical-fiber-based in-home optical networks," *IEEE Communications Magazine*, vol. 52, no. 6, pp. 186–193, 2014.

[3] S. Rajbhandari, J. J. McKendry, J. Herrnsdorf, H. Chun, G. Faulkner, H. Haas, I. M. Watson, D. OBrien, and M. D. Dawson, "A review of gallium nitride LEDs for multi-gigabit-per-second visible light data communications," *Semiconductor Science and Technology*, vol. 32, no. 2, p. 023001, 2017.

[4] X. Li, N. Bamiedakis, J. Wei, J. J. McKendry, E. Xie, R. Ferreira, E. Gu, M. D. Dawson, R. V. Penty, and I. H. White, "μLED-based Single-Wavelength Bi-directional POF Link with 10 Gb/s Aggregate Data Rate," *Journal of Lightwave Technology*, vol. 33, no. 17, pp. 3571–3576, 2015.

[5] F. Forni, Y. Shi, H. van den Boom, E. Tangdiongga, and T. Koonen, "Multiband LTE-A and 4-PAM signals over large-core plastic fibers for in-home networks," *IEEE Photonics Technology Letters*, vol. 28, no. 20, pp. 2281–2284, 2016.

[6] M. Atef and H. Zimmermann, *Optical Communication over Plastic Optical Fibers: Integrated Optical Receiver Technology*. Springer, 2012, vol. 172.

[7] R. Kruglov, S. Loquai, C.-A. Bunge, M. Schueppert, J. Vinogradov, and O. Ziemann, "Comparison of PAM and CAP modulation schemes for data transmission over SI-POF," *IEEE Photonics Technology Letters*, vol. 25, no. 23, pp. 2293–2296, 2013.

[8] H. Elgala, R. Mesleh, and H. Haas, "Non-linearity effects and predistortion in optical OFDM wireless transmission using LEDs," *International Journal of Ultra Wideband Communications and Systems*, vol. 1, no. 2, pp. 143–150, 2009.

[9] M. Schueppert, R. Kruglov, S. Loquai, and C.-A. Bunge, "Nonlinearities originated in a red RC-LED and Their impact on spectrally efficient modulation," *IEEE Photonics Technology Letters*, vol. 27, no. 19, pp. 2007–2010, 2015.

[10] K. Burse, R. Yadav, and S. Shrivastava, "Channel equalization using neural networks: a review," *IEEE Transactions on Systems, Man, and Cybernetics, Part C (Applications and Reviews)*, vol. 40, no. 3, pp. 352–357, 2010.

[11] E. Giacoumidis, S. T. Le, I. Aldaya, J. Wei, M. McCarthy, N. Doran, and B. Eggleton, "Experimental comparison of artificial neural network and volterra based nonlinear equalization for CO-OFDM," in *Optical Fiber Communications Conference and Exhibition (OFC), 2016*. IEEE, 2016, pp. 1–3.

[12] S. Gaiarin, X. Pang, O. Ozolins, R. T. Jones, E. P. Da Silva, R. Schatz, U. Westergren, S. Popov, G. Jacobsen, and D. Zibar, "High speed PAM-8 optical interconnects with digital equalization based on neural network," in *Asia Communications and Photonics Conference*. Optical Society of America, 2016, pp. AS1C–1.

[13] J. Mateo, M. Losada, and J. Zubia, "Frequency response in step index plastic optical fibers obtained from the generalized power flow equation," *Optics Express*, vol. 17, no. 4, pp. 2850–2860, 2009.

[14] G. Keiser, *Optical fiber communications*. Wiley Online Library, 2003.

[15] F. Breyer, *Multilevel transmission and equalization for polymer optical fiber systems*. Verlag Dr. Hut, 2010.

[16] J. Mateo, M. A. Losada, I. Garcés, and J. Zubia, "Global characterization of optical power propagation in step-index plastic optical fibers," *Optics express*, vol. 14, no. 20, pp. 9028–9035, 2006.

[17] M. C. Jeruchim, P. Balaban, and K. S. Shanmugan, *Simulation of communication systems: modeling, methodology and techniques*. Springer Science & Business Media, 2006.

[18] J. G. Proakis and M. Salehi, *Digital communications*. McGraw-Hill, 2008.

[19] J. Lee and V. J. Mathews, "A fast recursive least squares adaptive second order Volterra filter and its performance analysis," *IEEE transactions on signal processing*, vol. 41, no. 3, pp. 1087–1102, 1993.

[20] S. O. Haykin, *Neural networks and learning machines*. Pearson Upper Saddle River, NJ, USA:, 2009, vol. 3.

[21] P. S. Diniz, *Adaptive filtering*. Springer, 1997.

[22] P. A. Haigh, Z. Ghassemlooy, S. Rajbhandari, I. Papakonstantinou, and W. Popoola, "Visible light communications: 170 Mb/s using an artificial neural network equalizer in a low bandwidth white light configuration," *Journal of Lightwave Technology*, vol. 32, no. 9, pp. 1807–1813, 2014.

[23] S. Lim and C. Eun, "Predistorter design for a memory-less nonlinear high power amplifier using the pth-order inverse method for OFDM systems," in *Intelligent Signal Processing and Communication Systems, 2005. ISPACS 2005. Proceedings of 2005 International Symposium on*. IEEE, 2005, pp. 217–220.